Proceedings of the ASME 2010 3rd Joint US-European Fluids Engineering Summer Meeting and 8th International Conference on Nanochannels, Microchannels, and Minichannels
FEDSM-ICNMM2010
August 1-5, 2010, Montreal, Canada

FEDSM-ICNMM2010-30874

VALIDATION OF HEAT TRANSFER PERFORMANCE OF ELECTRICAL SUBMERSIBLE MOTOR USING CFD

Roshani O'Bryan, PhD
Baker Hughes - Centrilift
Claremore, OK, USA

Ketan Sheth
Baker Hughes - Centrilift
Claremore, OK, USA

Bruce Brookbank, PhD
Baker Hughes - Centrilift
Claremore, OK, USA

ABSTRACT

In oil field applications, the Electrical Submersible Pumping (ESP) unit (comprised of multistage pump, seal and motor) is placed inside a wellbore to provide necessary energy to lift reservoir fluids from the formation to the surface when the energy in the reservoir is not sufficient to lift the fluid to the surface. ESP motors produce heat while operating. The motors are cooled by the well fluid that passes the motor while being pumped. Many well fluids have very limited heat carrying capacity, resulting in higher operating temperature within the motor.

Only a limited number of studies have been conducted that have analyzed the inside temperature rise in the motor. A parametric study has been conducted using the computational fluid dynamic software Ansys CFX to examine the profile of the temperature rise in the motor. The computational model is validated by experimental data which showed that the computational model predicts the temperature with 95% accuracy. Therefore, this computational model effectively represents the experimentally determined temperature distribution of the motor.

INTRODUCTION

An Electrical Submersible Pumping (ESP) system incorporates a motor, seal section, and pump as shown in **Fig. 1**. The centrifugal pump, adds energy to the fluid which is used to make the fluid flow.

In oilfield applications, the ESP unit is placed inside a wellbore to provide necessary energy to lift reservoir fluids from the formation to the surface when natural energy in the reservoir is not sufficient. ESP motors produce heat while operating. This heat is removed by convection to the wellbore production fluids flowing past the motor. During the ESP operation, the fluids extracted from the reservoir are forced to flow past the motor and seal section in the annulus between those components and the wellbore. The fluid flow then enters the centrifugal pump, which adds energy (head) to the flow. The centrifugal pump discharges into tubing string that carries the extracted fluids to the surface.

According to Brown [1] the system design should maintain an ideal fluid velocity of 1 ft/s past the motor. This rule is based on the equation $Q = mC_p\Delta T$, which implies that the whole mass of the fluid flowing past the motor at any given instance absorbs all the heat generated inside the motor. In reality, a boundary layer develops and limits the amount of heat absorbed by the fluid. In the 1960's and 1970's most ESP installations were lower horsepower in wells having high API gravity (low density), high water cut fluids under 200° F [2–4]. The last twenty years, ESPs are being used in the high temperature, (greater than 350° F), high pressure applications where internal motor temperature is subjected to new limits and therefore, thermal modeling of the motor is required. Thermal study was also required to maintain electrical and mechanical component integrity and run life requirement.

HISTORY & LITERATURE REVIEW

Powers [5] addressed the lack of reality of this approach, and proposed more robust design criteria. He proposed that the motor winding temperature be calculated, based on heat transfer considerations and then compared to the manufacture's rating for the maximum allowable operating temperature. According to Powers, the motor winding temperature T_w is given by the following equation:

$$T_w = T_a + \Delta T_f + \Delta T_t + \Delta T_w \quad \textbf{(Eq. 1)}$$

Researchers [6-8] use the finite-element method (FEM) to estimate the temperature of the induction motor. This method is well suited for heat conduction problems. This method takes advantage of thermal asymmetry and is suited for solving steady state and transient problems. The CFD can handle three-dimensional and time-dependent problems involving complex geometry and multiple boundary conditions better than FEM. Additionally CFD provides more flexibility than FEM for the complex problems like heat rise in combined field of electrical and fluids.

Okoro [9] and Mellor [10] used the lumped-parameter thermal model to predict the temperature within an induction motor as well. Okoro used the system of nonlinear ordinary differential equation and algebraic equations which describe the thermal behavior of the system. The steady-state and transient temperature distributions were solved numerically using the Gauss-Siedel and the fourth-order Runge-Katta method.

Time-dependent lumped parameter thermal model of induction motor was developed [11]. Compared to finite element simulation of the heat transfer and fluid dynamic behavior of a motor during operation, in the lumped-parameter thermal model the fluid and solid components of the motor are lumped into relatively few, typically 10-100, isothermal nodes. These nodes are then coupled with appropriate heat transfer expressions, representing conduction and convection heat transfer between nodes. Bogliett [12] compared the strengths and weaknesses of lumped-parameter and finite element analysis for thermal modeling electrical machines.

Heat transfer from ESP motors is by forced convection where the thermophysical properties of the fluid and the flow velocity determine the heat transfer coefficient. Using dimensional analysis, these fluid characteristics are grouped into three dimensionless "numbers" that can be used to effectively predict heat transfer rates and subsequently motor operating temperatures. These dimensionless entities are the Reynolds Number, Prandtl Number and Nusselt Number, named for the individuals who developed them.

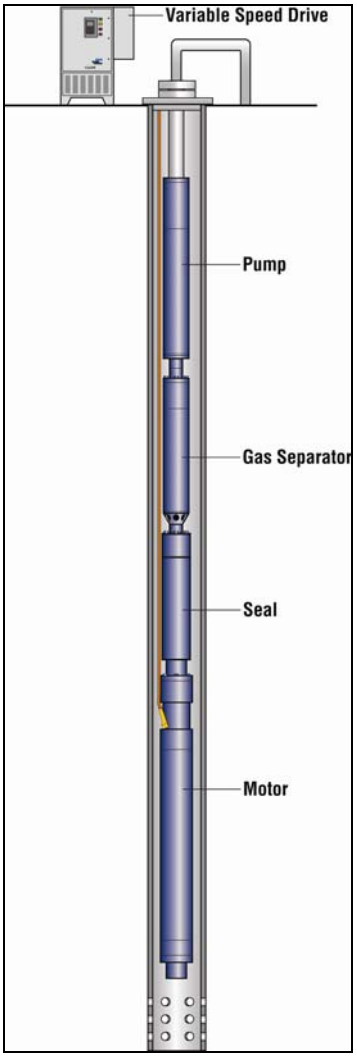

Fig. 1 Typical ESP system

Dimensionless Numbers

First, we will explore the effect of the dimensionless number and then individual properties in details as follows:

Three dimensionless numbers are defined as:

Reynolds Number $\mathrm{Re} = \rho VL / \mu$

Prandtl Number $\mathrm{Pr} = \mu Cp / k$

Nusselt Number $Nu = hL / k$

Reynolds Number Effect: The Reynolds Number is the ratio of inertial forces to viscous forces in a flowing fluid. Fluid flow regime is based on Reynolds Number. For fluid friction considerations for a flow in a pipe and an annulus, three regions are: Laminar region for RE < 2300; Transitional region for 2300 < RE < 4000 and Turbulent region for RE > 4000. These limits are defined to calculate fluid friction losses only and these limits are not applicable for heat transfer region considerations. The heat transfer region is based on Reynolds number as: Laminar region for RE < 2300; Transitional region for 2300 < RE < 10000 and Turbulent region for RE > 10000 [13, 14].

Heat transfer is very efficient in the turbulent flow regime and very poor in the laminar flow regime for a pipe and an annulus area. The turbulent flow as implied by its name mixes the fluid so that heat transfer is accomplished by conduction through the fluid and by physically moving hot fluid away from the surface of the ESP and replacing it with cooler fluid. In other words, the turbulent flow is more efficient for the heat transfer and the motor cooling

	Friction Losses	Heat Transfer
Laminar region	RE < 2300	RE < 2300
Transitional region	2300 < RE < 4000	2300 < RE < 10000
Turbulent region	RE > 4000	RE > 10000

Table 1. Flow Region

Detailed research has been reported [13–15] for a pipe flow for heat transfer. However, heat transfer for laminar flow in eccentric annular areas has not been extensively studied. One has to derive a generalized model for predicting heat transfer based on assumptions. This leads to approximate results.

Prandtl Number Effect: The Prandtl Number is a ratio of kinematic viscosity to the thermal diffusivity of the fluid. The practical effect is that for a given Reynolds Number, fluids with high Prandtl Numbers (low gravity, higher viscosity crude oils) will have a high temperature gradient across the convective film at heat transfer surfaces with subsequent lower heat transfer rates. Fluids with lower Prandtl Numbers (water and high water cut fluids) will have higher heat transfer rates.

Nusselt Number Effect: The Nusselt number is the ratio of convective conductance (“h”, film coefficient) to molecular conductance (thermal conductivity) over the hydraulic diameter (k/Dh)or h*Dh/k. The Nusselt Number has a direct effect on cooling based on Reynolds Number. In laminar flow heat transfer (RE < 2300), the Nusselt number is nearly constant, and therefore has not been researched in detail. The Nusselt number in Transitional flow heat transfer (for 2300 < RE < 10000) has less research. Generally, heat transfer for laminar flow and turbulent flow is calculated and then averaged for transitional flow heat transfer. Detailed studies have been completed and accurate models are available for turbulent flow heat transfer (RE >10000), including a complete range of Prandtle Numbers and eccentricity [14]

Thermophysical Properties

These dimensionless numbers are a function of four thermophysical properties and one fluid mechanics property. These are the fluid: specific heat, viscosity, density, thermal conductivity and flow velocity.

Viscosity: Viscosity is a measure of the internal friction within a fluid. It relates the shear stress between the stream lines of a flowing fluid to the change in the flow velocities between the stream lines. For constant velocity fluid flow, As viscosity increases, the flow moves from turbulent flow to transitional flow to laminar flow. As viscosity increases, the internal fluid friction and friction losses increas. For liquids, viscosity is inversely proportional to temperature, and directly proportional with the pressure. Viscosity is more sensitive to temperature variations than pressure variations. Reynolds Number is inversely proportional to viscosity. A low viscosity fluid (water) will develop turbulence and cross flow that results in higher heat transfer rates at lower velocities.

Velocity: Velocity increases in the direct proportion of the flow rate for a given application. Friction losses vary with square of the velocity. Therefore, at a fixed point, friction losses increase as the square of the flow rate. Reynolds Number increases in direct proportional to velocity. Friction losses increase by square ratio with an increase in Reynolds Number.

In larger diameter casing, velocity can be increased by shrouding the motor. Shrouding the motor is very common when an ESP is set below the perforations in gassy applications

Velocity has a very small effect in the laminar flow region. The motor internal temperature increases with motor load in a constant velocity condition. The motor internal operating temperature increases with an increase in the ambient fluid temperature. Viscosity did not have an effect on motor temperature for viscosities over 100 Cp as the flow was laminar. . Figure 2- 3 represents the effect of velocity on the motor internal temperature with different loading conditions.

Density: Density is the weight per unit volume. Generally, crude oil is lighter than water, and the lighter the oil, the lower the viscosity. A flowing, dense fluid will

have higher inertial forces to overcome the drag of viscous forces. Turbulence is more easily developed with higher heat transfer rates. Water is denser than oils and water cools ESP motors better than crude oils. Gas in crude oil reduces density two ways. Gas bubbles and dissolved gas reduce the mass per cubic foot. Gas in the solution also makes the oil less viscous. As crude oil pressure decreases, solution gas comes out of the fluid resulting in a heavier liquid phase. This increases density and viscosity of the liquid phase. Reynolds number is directly proportional to the density of the crude oil.

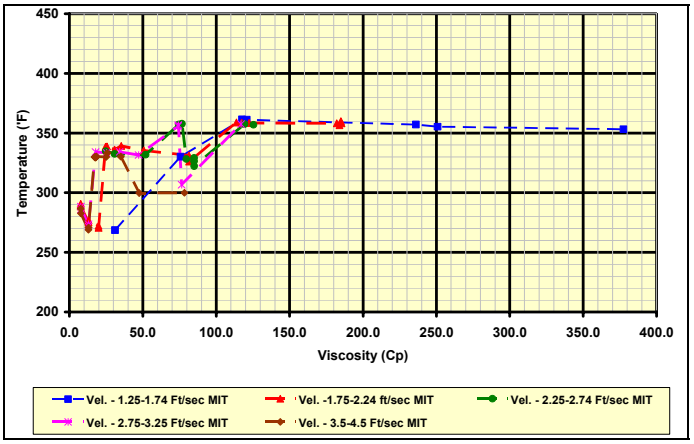

Fig.2 Effect of Velocity on motor internal temperature at 110% loading

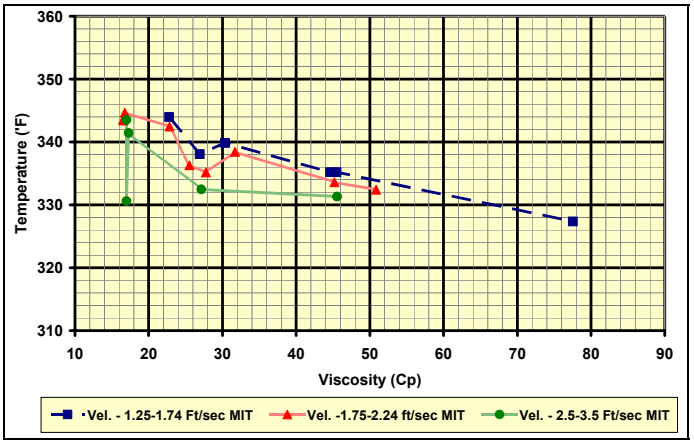

Fig. 3 Effect of Velocity on motor internal temperature at 90% loading

Density: Density is the weight per unit volume. Generally, crude oil is lighter than water, and the lighter the oil, the lower the viscosity. A flowing, dense fluid will have higher inertial forces to overcome the drag of viscous forces. Turbulence is more easily developed with higher heat transfer rates. Water is denser than oils and water cools ESP motors better than crude oils. Gas in crude oil reduces density two ways. Gas bubbles and dissolved gas reduce the mass per cubic foot. Gas in the solution also makes the oil less viscous. As crude oil pressure decreases, solution gas comes out of the fluid resulting in a heavier liquid phase. This increases density and viscosity of the liquid phase. Reynolds number is directly proportional to the density of the crude oil.

Specific heat: Specific heat is a measure of how much heat is required to raise the temperature of a unit mass of a fluid by one degree of temperature. It is a measure of the heat carrying capacity of a flowing fluid. The Prandtl Number is directly proportional to the specific heat.

Thermal conductivity: Thermal conductivity is the time rate at which a fluid can conduct heat through a unit area with a unit thickness for a unit temperature difference. The thermal conductivity of water is more than four times greater than oils. Prandtl and Nusselt Numbers vary inversely with thermal conductivity.

These two are very important properties affecting motor cooling. In fluids, heat is transferred via the conduction and convection process. Heat is transferred to the fluid in the boundary layer through conduction and then to the rest of the fluid by convection.

The coefficient of thermal conductivity represents the rate of heat transfer by conduction from a unit area on one side of a solid or static liquid to an equal area on the other side of the solid or static liquid one unit length apart for a temperature change of 1°. Oil is a poor conductor of heat, and has a substantially lower coefficient of thermal conductivity than water.

Table 2 summarizes these properties for water and oil. Both, specific heat and the coefficient of thermal conductivity are temperature dependent. Generally, the temperature dependence of the properties is ignored.

	Friction Losses	Heat Transfer
Laminar region	RE < 2300	RE < 2300
Transitional region	2300 < RE < 4000	2300 < RE < 10000
Turbulent region	RE > 4000	RE > 10000

Table 1. Flow Region

ESP Motor

Typically for ESP applications, an AC three-phase induction motor is used due to its simplicity and ruggedness. Its purpose is to convert electricity energy into rotating mechanical energy.

Motor Components: The two main electromagnetic components of an AC three-phase induction motor are the stator and the rotor. The stator is made by stacking several thin laminations stamped from sheet metal with low magnetic losses.

The lamination is punched with several slots. For a three-phase motor, three windings made of insulated wire are inserted within these slots. Insulation and bedding materials such as epoxy or varnish are injected into the stator slots as shown in Fig. 4.

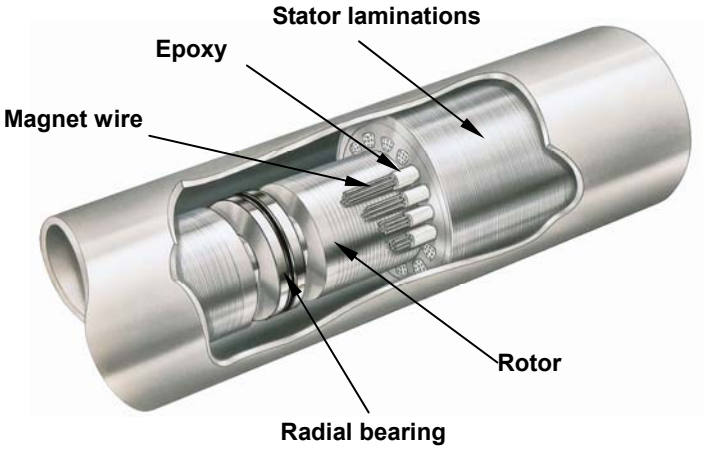

Fig. 4 Motor components

The rotor is constructed in a similar way. It is also a stack of several thin sheets of magnetic material called rotor lamination. The rotor lamination is also punched with several holes. These rotor holes are filled with copper rotor bars. These rotors bars are short-circuited at their ends by two conducting end rings. The rotating magnetic field from the stator induces a current in the rotor bars. A force is generated between the magnetic field and the rotor bar that causes the torque and rotation of the rotor. Motor oil is used to fill all internal space inside the motor. This motor oil fills the “air” gap between the rotor and stator. The motor oil is equalized with the pressure in the well bore so that the motor does not require heavy wall housing or high pressure joints.

Mathematical Presentation of an Induction Motor

Equivalent Circuit: For steady-state operation, **Fig. 5** illustrates the per-phase mathematical representation of an AC induction motor [8]. As voltage (VT) is applied to the stator windings, the current (I1) flows through stator resistance and the stator reactance. The current (IM) flows through the mutual reactance and the iron loss resistance. The other current, I2, is the induced rotor current that flows through the rotor resistance and the rotor reactance. As the currents, I1, IM and I2, flow through the various motor parts, several power components are created.

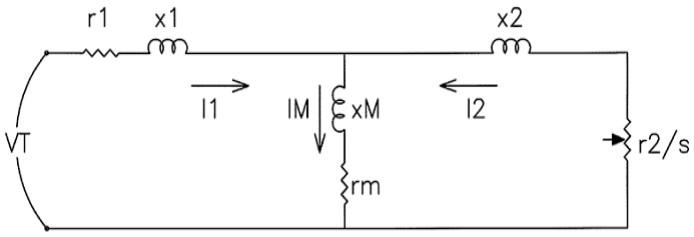

Fig. 5 Equivalent circuit of an AC induction motor

The power flow in an AC induction motor is then described as shown in Fig 6. The stator power loss creates heat in the stator winding. The iron loss creates heat in the stator lamination. Similarly, the rotor loss generates heat in the rotor bars. Finally, the friction & fluid loss generates heat in the bearings and in the motor oil in the “air” gap inside the motor.

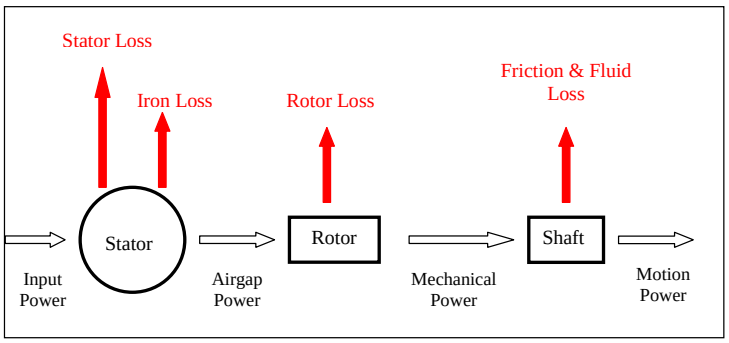

Fig. 6 Power flow in the AC induction motor

Computational Approach

This parametric study was conducted using the computational fluid dynamic software Ansys CFX. version 12. This software provides finite volume element simulation of system flow geometry and solves the Navier Stokes equation. Fig. 7 represents a schematic of a two-dimensional cross section of the 725 series submersible motor consider in this study. The mean out side diameter of the motor is 7.25 in.

A ¼ section of the motor is used as the model, taking advantage of the symmetry of the motor. Fig. 8 represents the CFX model of the motor.

The computational simulation was conducted assuming, steady-state, incompressible flow conditions. The flow of

oil in the “air” gap between rotor and stator is laminar flow. The rotor is rotating at 3500 rpm. The copper wire winding of the stator in the motor occupied the 65% stator slot area, which is represented by randomly placed copper lumped mass. The remainder of the slot is filled with varnish or epoxy

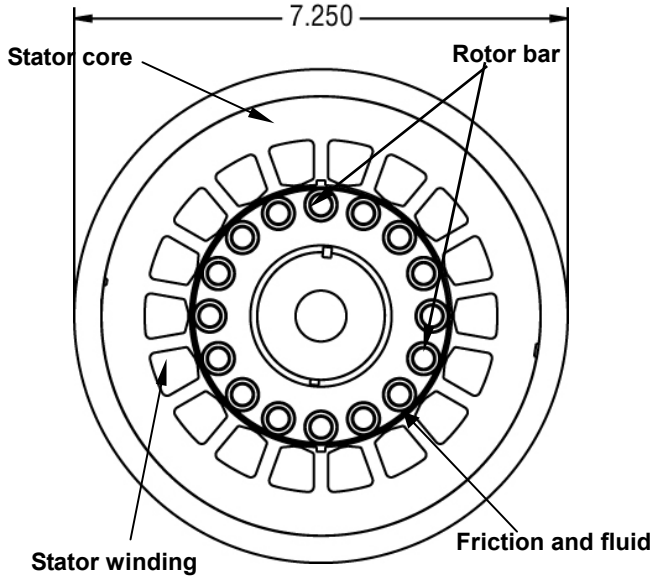

Fig. 7 725 Series motor cross section

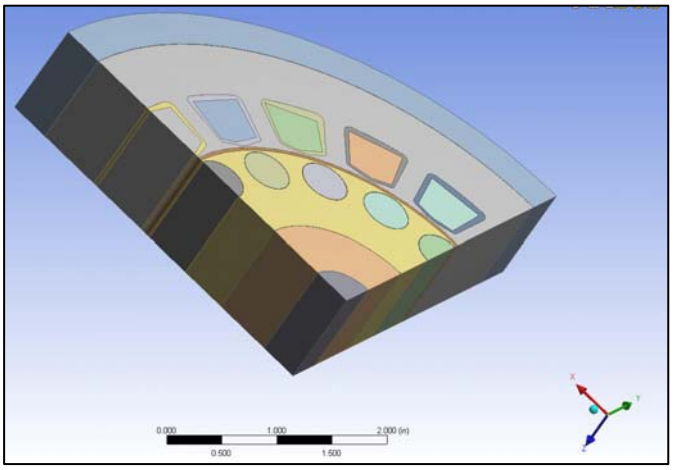

Fig. 8 Quarter section of the motor

The heat generated by rotor bar, stator winding, fluid and stator core was modeled as a uniform heat flux (constant heat source) in the model. The constant motor housing temperature was used as a steady state condition in the outer wall of the motor housing. A Dell precision dual core 64 bit computer is used in this study.

Meshing

ESP motor consists with very fine oil gap between the following areas: stator and the rotor, housing and stator, shaft and rotor, rotor bars and rotor. In order to capture the boundary layer conditions, fine structured mesh was used in the oil gap area. In this case 2500 nodes are use in the oil gap region (of 0.011”). Other areas of the motor are meshed with an unstructured grid method. The model is first run with coarse mesh and then the mesh size was reduced until the solution was stable. In this model 5000 iterations were used to archive the desired convergence of the 5th order.

Experimental Model

In order to validate the computational model, it was compared with experimental data [16]. One 725 series, 200 HP, 4 rotors, 54 Amp, Centrilift XP motor was used in a horizontal layout, centered in 10.75” internal diameter casing (pod). The six thermocouples (at three locations, 180˚ apart) were embedded in the stator winding to measure the internal temperature of the motor. Motor external temperature was monitored at 10 locations from the bottom of the motor to the top of the motor.

Fig. 9 Centrilift Testing Facility

Fluid temperature was monitored at several locations. Synthetic oil with a viscosity range of 140 Cp to 15 Cp was used. Viscosity was controlled and measured by fluid temperature at the pod inlet. Fluid temperature was controlled with the help of a forced air heat exchanger. Figure 9 shows the test facility.

Results

The computational results provide the thermal behavior of the inside the motor. Figures 10 and 11 represents the

temperature contour map and the temperature profile obtained for 725 motor.

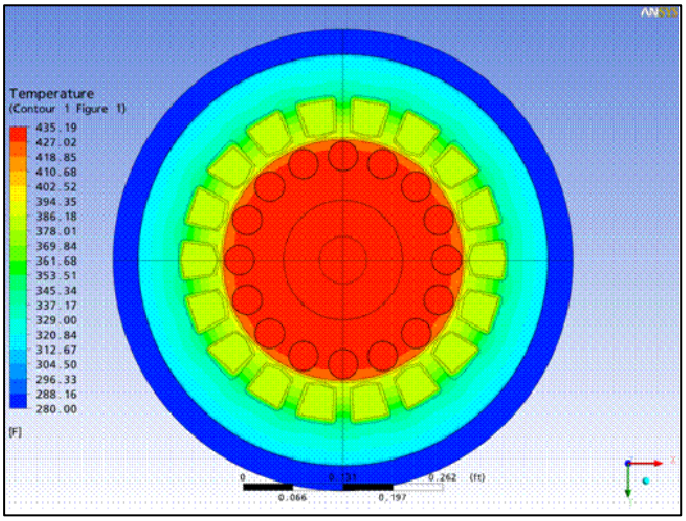

Fig. 10 Temperature contours in 725 motor

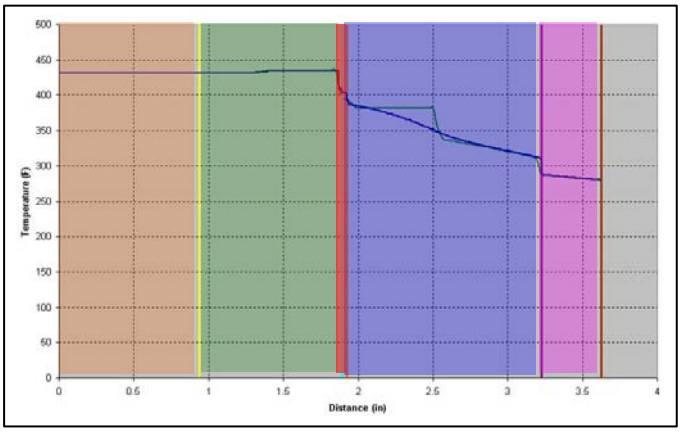

Fig. 11 Temperature profile across the 725 motor

Temperature profile with out magnetic wire
Temperature profile with magnetic wire

shaft rotor oil gap stator
housing

The numerical results are compared with the experimental data as shown in **table 3** for various motor loading and fluid temperatures. The experimental results indicate that the computational model predicts the temperature with 95% accuracy. The computational model effectively represents the experimental data. Figure 12 and 13 compares the measured motor internal temperature and simulated motor internal temperature for fluid temperature at 145^0F and 105^0F respectively.

Motor loading	Average fluid temperature (°F)	Average motor internal temperature (measured) (°F)	CFD predicted internal temperature (°F)	% Error
100%	104.361	361.37	376	4%
110%	102.571	357.80	366	2.24%
90%	142.183	361.99	378	4.5%
100%	145.210	363.27	381	4.6%
110%	144.046	358.94	374	4%

Table 3. Motor temperature comparison with loading

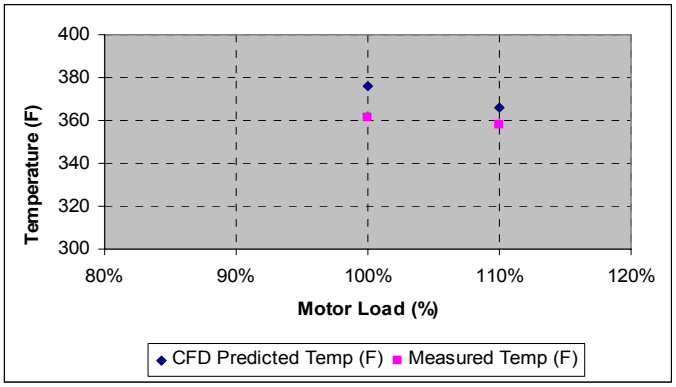

Fig. 12 Comparison of CFD & test data at fluid temperature of 105 F

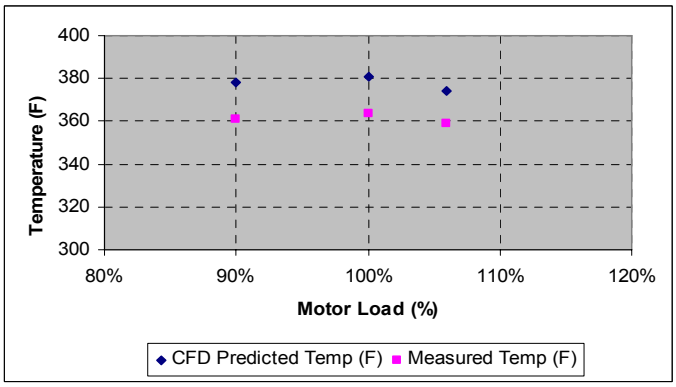

Fig. 13 Comparison of CFD & test data at fluid temperature of 145 F

Conclusion

The CFD model is developed, experimentally verified and applied to application. The experimental results presented in this paper show that the developed motor heat transfer model is capable of calculating the temperatures in the motor accurately at the rated loads. Accuracy of the results is within 95%. When the flow is laminar, velocity has a very small effect on the motor internal temperature.

ACKNOWLEDGMENTS

The authors would like to acknowledge Baker Hughes - Centrilift for permission to publish this paper, and Baker Hughes-Centrilift's technical publications group for helping with the preparation.

NOMENCLATURE

Re = Reynolds Number (dimensionless)

Pr = Prandtl Number (dimensionless)

Nu = Nusselt Number (dimensionless)

V = Velocity (Ft/Sec)

L = Characteristic Length (Ft)

h = Velocity (Ft/Sec)

k = Thermal Conductivity (Btu. Ft/ (hr. Ft2 . ° F)

Cp = Specific Heat (Btu/ (Lb . ° F)

ρ = Density (Lb/Ft3)

μ = Viscosity (Centipoise)

T_w = motor winding temperature

ΔT_f = fluid temperature increase

ΔT_s = fluid temperature difference between the produced fluid and the motor housing surface

ΔT_w = difference between the motor surface temperature and the winding temperature

VT = voltage applied to the motor

r1 = stator resistance

x1 = stator leakage reactance

xM = mutual reactance

rm = iron loss resistance

x2 = rotor reactance

r2 = rotor resistance

s = motor slip

I1 = stator current

IM = iron loss resistance current

I2 = rotor current

REFERENCES

1. Brown, Kermit E., “The Technology of Artificial Lift Methods,” PennWell Publishing, 1980.

2. Vandevier, J., “Electric Submersible Pumps in Geothermal Pumps in Geothermal Environment,” 1980

3. Vandevier, J., “Production of Geothermal Resources using Electric Submersible Pumps,” 1983

4. Vandevier, J., “High Temperature Electric Submersible Pumps,” 1982

5. Powers, Maston L., “Depth Constraint of Electric Submersible Pumps,” SPE 24835, May 1994.

6. Shaker, D., Mukherjee, P. K., and Sen, S. K. “Approximate Analysis of Steady State Heat Conduction in an Induction Motor,” IEEE Trans. Energy Convers., vol.8-1, pp 78-84, Mar. 1993

7. Griffith, J. W., McCoy, R. M., and Sharma, D. K., “Induction Motor Squirrel Cage Rotor Winding Thermal Analysis,” IEEE Trans. Energy Convers., vol.1-3, pp 22-25, Mar 1986.

8. Chan, C. C., Yan, L. Chen, P., Wang, Z., and Chau, K. T., “Analysis of Electromagnetic and Thermal Fields for Induction Motors during Starting,” IEEE Trans. Energy Convers., vol.9-1, pp 53-58, Mar. 1994.

9. Okoro, O. I., “Steady and Transient State Thermal Analysis of a 7.5kW Squirrel Cage Induction Machine at Rated Load Operation,” IEEE Trans. Energy Convers., vol.20-4, pp 730-736, Dec. 2005.

10. Mellor, P. H., Roberts, D. and Turner, D.R., “Lumped Parameter Thermal Model for Electrical Machines,” Proc. Inst. Elect. Eng., vol.138-ptB, no. 5, pp-205-218, 1995.

11. Jankowski, T., Prenger, C.F., Hills, D.D. O’Bryan, S.R. Sheth, K.K., Brookbank, E.B. Hunt, D.F. and Orrego, Y. A. “ Development and Validation of a Thermal Model for Electrical Induction Motor,” IEEE Trans. Industrial Electronics, vol

12 A. Boglietti, A. Cavagnino, D. Staton, M. Shanel, M. Mueller, and C. Mejuto, "Evolution and Modern Approaches for Thermal Analysis of Electrical Machines," IEEE Transactions on Industrial Electronics, vol. 56, pp. 871-882, 2009.

13. Shah, R. K., London, A. L., “Laminar Flow Forced Convection in Ducts,” Supplement I to *Advances in Heat Transfer*, Academic Press, New York, 1978

14. Rohsenow, W., Hartnett, J., Cho, Y., “Forced Convection, Internal Flow in Ducts,” Chapter 5, *Handbook of Heat Transfer*, McGraw- Hill, 3rd Edition, 1998

15. Shah, R. K., Bhatti, M. S., “Laminar Convection Heat Transfer in Ducts,” *Handbook of Single Phase Convective Heat Transfer*, Wiley-Interscience, John Wiley & Sons, New York, 1987

16. Sheth, K., Synder, K.C., and Fox, M., “Verification of Motor Internal Heat (Temperature) Rise by AutographPC® Program,” 2007 (Internal document).

17. Skoczylas, P., Alahanti, F.J.S., “Flow Regime Effects on Downhole Motor Cooling,” SPE Gulf Coast ESP Workshop, 1998

18. Manzanilla, R., Moreno, N., Yanez, R., “Heat Transfer between Heavy Oil Flow & Electrical Submersible Pump Motor,” SPE Gulf Coast ESP Workshop, 1997